applied sciences

MDPI

Article

Route Optimization for Electric Vehicle Cold Chain Delivery Under a Mixed Public–Private Charging Mode: A China-Oriented Case Study

Yu Ji, Kaikai Su * and Chen Chen

College of Economics and Management, Tianjin University of Science and Technology, Tianjin 300222, China; 050429@mail.tust.edu.cn (Y.J.); 050830@mail.tust.edu.cn (C.C.)
* Correspondence: sukaikai@tust.edu.cn; Tel.: +86-15201328501

Abstract

This study addresses the electric refrigerated vehicle routing problem under a mixed public–private charging mode. An optimization model is developed with the objective of minimizing total cost. The model jointly considers vehicle load capacity, battery capacity, customer time windows, refrigeration energy consumption, cargo damage cost, and the heterogeneity of charging resources. To solve this NP-hard problem, an improved Grey Wolf Optimizer is proposed. The algorithm enhances solution quality and convergence performance through elite individual selection, a "destruction–repair" operator, and an adaptive position update strategy. Experimental results based on modified Solomon benchmark instances show that the proposed model can effectively capture the operational characteristics of electric refrigerated distribution under mixed charging scenarios. The proposed IGWO is compared with GA, GWO, and ALNS over multiple independent runs, and the results reported as means ± standard deviations demonstrate its competitive solution quality and robustness. These findings provide theoretical support for optimizing electric cold-chain distribution systems and coordinating charging resources.

Keywords: public private charging stations; electric vehicle routing problem (EVRP); improved gray wolf optimization (IGWO); cold chain delivery

1. Introduction

With the implementation of China's 15th Five-Year Plan and the continued advancement of the "dual carbon" strategy, electric cold-chain logistics has emerged as a key direction for enhancing agricultural product circulation, reducing food losses, and promoting low-carbon freight transportation. The Outline of the 15th Five-Year Plan emphasizes the improvement of agricultural product markets and circulation networks, as well as the development of warehousing, preservation, and cold-chain logistics systems [1]. From an economic perspective, cold-chain logistics is also expanding rapidly. According to data released by the China Federation of Logistics and Purchasing at the 17th Global Food Cold Chain Conference, the global cold-chain logistics market reached approximately USD 363.8 billion in 2024, with China accounting for more than 20% of the global market. In the first half of 2025, China's food cold-chain logistics demand reached approximately 192 million tons, representing a year-on-year increase of 4.35%. Meanwhile, the total logistics value reached approximately CNY 4.7 trillion, representing a 4.21% year-over-year increase [2]. Nevertheless, China's fresh agricultural product circulation still faces relatively

Academic Editor: Arkadiusz Gola

Received: 21 April 2026
Revised: 7 May 2026
Accepted: 8 May 2026
Published: 9 May 2026

high loss pressure. According to the Ministry of Agriculture and Rural Affairs of China, the cold-chain transportation rates of fruits and vegetables, meat, and aquatic products in China are 35%, 57%, and 69%, respectively, while the average level in developed countries exceeds 90%; taking meat as an example, the circulation loss rate in China is about 12%, compared with only 3% in the United States [3]. Therefore, improving cold-chain logistics efficiency has important implications for reducing cargo losses, ensuring food safety, and lowering distribution costs.

The electrification of freight vehicles and the rapid expansion of charging infrastructure further provide practical conditions for the development of electric cold-chain logistics. According to the International Energy Agency's Global EV Outlook 2025, global sales of electric medium- and heavy-duty trucks exceeded 90,000 units in 2024, increasing by nearly 80% year on year, with more than 80% sold in China [4]. In China's commercial vehicle sector, new-energy commercial vehicle registrations increased from about 333,000 in 2023 to 546,000 in 2024, and the penetration rate rose from 11.3% to 19.0% [5]. In the refrigerated transport sector, China Daily reported that 29,474 refrigerated trucks were sold in China in the first half of 2025, up 18.19% year on year; among them, sales of new-energy refrigerated trucks reached 10,548 units, up 119.61% year on year, and their market penetration rate reached 35.8% [6]. Meanwhile, China's charging infrastructure has continued to expand rapidly. According to the National Energy Administration, by the end of March 2026, the total number of EV charging facilities in China had reached 21.481 million, including 4.863 million public charging facilities and 16.618 million private charging facilities [7]. In addition, China's Three-Year Action Plan for Doubling EV Charging Service Capacity proposes that, by the end of 2027, 28 million charging facilities will be built nationwide, providing more than 300 million kW of public charging capacity and meeting the charging demand of more than 80 million electric vehicles [8]. These developments indicate that electric refrigerated distribution has entered a stage of rapid application, but its operational efficiency still depends on the coordinated optimization of routing, battery energy consumption, refrigeration demand, and charging resource selection.

Existing studies also support the need for integrated optimization in this field. Cold-chain distribution route optimization generally needs to consider transportation cost, refrigeration cost, cargo damage, carbon emissions, and customer time-window constraints [9]. More specifically, logistics distance has been recognized as an important factor influencing transport-related carbon emissions. The concept of food miles emphasizes that the spatial separation between food production and consumption affects the carbon footprint of food supply chains. Lee and Stoeltje [10] estimated food transportation distances and associated CO_2 emissions across highway networks, showing that road-based logistics distance is closely related to the carbon burden of food distribution. From the perspective of freight vehicle decarbonization, Maggini et al. further demonstrated that the technical and economic performance of zero-carbon road freight vehicles is strongly associated with mileage, energy consumption, and operating conditions [11]. These studies indicate that reducing unnecessary travel distance and improving route efficiency are important not only for lowering distribution costs but also for reducing transport-related emissions.

Compared with conventional cold-chain logistics, electric cold-chain distribution further involves the coupling of driving energy consumption, refrigeration energy consumption, temperature-controlled delivery requirements, and soft time-window constraints [12]. In addition, charging decisions have a significant influence on electric vehicle routing, since the state and availability of charging stations affect route feasibility, charging timing, and overall distribution cost [13]. The rapid expansion of charging infrastructure provides practical support for EV deployment, but also creates new challenges related to infrastructure planning, charging accessibility, and energy coordination [14]. Therefore, electric cold-chain vehicle scheduling under mixed charging conditions requires a more integrated modeling framework that jointly considers routing, freshness preservation, charging constraints, and heterogeneous charging resources [15]. Furthermore, due to constraints such as driving range, battery capacity, charging time, and charging infrastructure conditions, the electric vehicle routing problem is no longer a simple extension of the classical vehicle routing problem. It has evolved into an electric vehicle routing problem (EVRP) that requires integrated decisions on routing, energy consumption, and recharging strategies [16–21]. Existing studies have explored extensions involving time windows, partial recharging, satellite customers, and heterogeneous fleets, driving EVRP research from basic feasibility models toward more realistic and comprehensive operational optimization problems [16–18,20–22].

As research progresses, scholars have increasingly focused on the real energy consumption characteristics of electric vehicles during operation. Existing studies show that energy consumption is not only related to travel distance, but is also jointly affected by traffic congestion, vehicle load, operating speed, and the charging process [23–28]. Therefore, time-dependent traffic conditions, load–speed coupling effects, nonlinear charging functions, and energy consumption uncertainty have become key directions in refined EVRP modeling [23–27]. At the same time, some studies incorporate public charging stations, mobile battery swapping, and charging station heterogeneity into routing optimization frameworks. These works suggest that recharging decisions have evolved from a simple "whether to charge" choice to a comprehensive decision problem involving when, where, and at what cost to use different types of charging resources [29–33].

Compared with conventional distribution, cold-chain logistics must additionally consider refrigeration energy consumption, cargo damage costs, and the impact of service time on product quality [34–36]. Existing studies indicate that the cost structure of cold-chain distribution exhibits strong multidimensional coupling [34,36]. Models based solely on travel distance or driving energy consumption cannot accurately represent real-world operations. In particular, in electric cold-chain distribution scenarios, vehicle driving energy consumption, refrigeration load, customer time windows, and recharging strategies interact with each other, further increasing the complexity of the problem [34,35].

In terms of solution methods, as the number of constraints increases and the level of coupling becomes more complex, the applicability of traditional exact algorithms to medium- and large-scale problems is limited. Metaheuristic algorithms and their hybrid improved variants have therefore become a major research focus [37–41]. Although existing studies have made progress in improving solution efficiency and solution quality, several issues remain in complex scenarios, such as poor initial solution quality, limited local search capability, and a tendency to fall into local optima [37–40].

In summary, existing research still has limitations in several aspects, including insufficient representation of differences between public and private charging resources [42–44], lack of systematic analysis of the interaction among driving energy consumption [34–36], refrigeration energy consumption, and recharging decisions, and room for improvement in solution methods under complex constraints [37–40]. Against this background, this paper focuses on electric refrigerated vehicle routing for cold-chain logistics enterprises under a mixed public–private charging mode. An optimization model is developed with the objective of minimizing total cost. The model integrates fixed vehicle costs, transportation costs, charging costs, refrigeration costs, cargo damage costs, and time-window penalty costs within a unified framework. Meanwhile, given the complexity of the constraints and the difficulty of solving the model, an improved Grey Wolf Optimizer is proposed. The algorithm improves solution performance through elite individual selection, a "destruction–repair" mechanism, and an adaptive position update strategy. This study provides theoretical support for optimizing electric cold-chain distribution systems under mixed charging scenarios and offers practical guidance for enterprise charging strategies and distribution planning decisions.

Compared with existing EVRP and cold-chain routing studies, the main contributions of this study are fourfold.

First, this study develops an electric refrigerated vehicle routing model under a mixed public–private charging mode. Unlike studies that treat charging resources as homogeneous, this model explicitly distinguishes public and private charging stations in terms of charging cost, charging power, and charger availability, thereby better reflecting the operational characteristics of real mixed charging scenarios.

Second, this study integrates the operational characteristics of electric cold-chain delivery into a unified cost-minimization framework. The model jointly considers vehicle fixed cost, transportation cost, charging cost, refrigeration cost, cargo damage cost, and time-window penalty cost. In addition, SOC-dependent nonlinear charging, charging-station queuing, and link-based time-dependent travel time are incorporated to capture the coupling relationship among routing decisions, charging behavior, refrigeration operation, and traffic conditions.

Third, an improved Grey Wolf Optimizer is proposed to solve the highly constrained electric refrigerated vehicle routing problem. The proposed algorithm improves the standard GWO through high-quality initial individual selection, a destroy–repair operator, and an adaptive position update strategy, aiming to enhance initial solution quality, local search capability, and the balance between global exploration and local exploitation.

Fourth, the effectiveness and robustness of the proposed model and algorithm are evaluated through numerical experiments based on modified Solomon benchmark instances. Multiple independent runs, mean and standard deviation statistics, comparison with GA, GWO, and ALNS, and sensitivity analyses of key parameters are conducted to provide more reliable evidence for the performance of the proposed approach.

These contributions provide methodological support for electric cold-chain vehicle routing optimization and offer practical implications for logistics enterprises in coordinating delivery routes, charging decisions, and public–private charging resources under low-carbon transportation scenarios.

2. Materials and Methods

This paper first clearly defines the cold chain delivery route optimization problem, specifying the system boundaries and core decision factors. On this basis, it identifies the key constraints and optimization objectives by considering the operational characteristics of electric vehicles and the differences in charging infrastructure.

2.1. Problem Description

A cold chain delivery company operates a distribution center and a fleet of electric delivery vehicles. All vehicles depart from the distribution center, complete their delivery tasks, and return to the center. Within the delivery area, there are several private and public charging stations. Private charging stations charge a fixed electricity rate, while public stations charge a combination of a base rate and a service fee, with additional variable electricity costs. The energy consumption of each electric refrigerated vehicle is affected not only by vehicle load and travel speed, but also by road gradient, stop-and-go traffic conditions, and ambient temperature. In particular, road gradient and traffic interruptions influence driving energy consumption, while ambient temperature affects both traction energy use and refrigeration demand. Therefore, this study extends the original load–speed-based energy consumption function by incorporating these real-world operating factors.

The charging process is no longer simplified as a linear process with constant charging power. In practical EV operations, the charging power varies with the vehicle's state of charge (SOC), and charging speed usually decreases when the battery approaches a high SOC range. Moreover, vehicles may not be able to start charging immediately after arriving at a charging station because chargers are limited and may be occupied by other vehicles. Therefore, this study incorporates an SOC-dependent nonlinear charging function and a shared-charger queuing mechanism to better describe the charging process under mixed public–private charging conditions.

Instead of using a global constant speed for different time periods, this study further constructs a link-based time-dependent travel time model. Each road link is assigned its own distance, free-flow speed, basic capacity, and storage limitation. During peak periods, link speed and link capacity are reduced to reflect traffic congestion. When the number of vehicles on a link reaches its storage capacity, subsequent vehicles must wait upstream, thereby capturing congestion propagation and spillback effects. Customers served by the company have explicit time window constraints. Vehicles must arrive and complete deliveries within the specified time periods. Arriving earlier or later incurs additional costs. Considering constraints such as link-based time-dependent travel time, vehicle load, battery capacity, SOC-dependent charging time, charging station queuing, and customer time windows, the goal is to minimize the total cost by jointly optimizing charging station selection and delivery routes.

2.2. Modeling Conditions and Assumptions

To facilitate problem modeling and algorithm design, the following assumptions are made:

Assumption 1. *Delivery routes are closed, and goods flow in a single direction only.*

Assumption 2. *Vehicle speed varies by road link and time period, and is determined by the link-based time-dependent travel time model.*

Assumption 3. *Vehicle travel time is link-dependent and time-dependent. Each road link has its own free-flow speed, basic capacity, and storage limitation. During peak periods, both link speed and link capacity may decrease, and vehicles may experience upstream waiting when the storage capacity of a link is reached.*

Assumption 4. *Public and private charging stations differ in charging power, charging cost, and charger availability. The charging power is determined by the station type and the vehicle's current SOC level.*

Assumption 5. *A non-split delivery policy is adopted. Each customer must be visited exactly once by a single vehicle, and the full demand of that customer must be delivered during that visit.*

Assumption 6. *EV energy consumption depends on vehicle weight, real-time load, travel speed, travel distance, road gradient, stop-and-go traffic conditions, and ambient temperature. The effects of road gradient and traffic conditions are reflected in the driving energy consumption function, while the effect of ambient temperature is incorporated into both driving and refrigeration energy consumption.*

Assumption 7. *Charging costs differ between private and public stations. Vehicles can prioritize charging or traveling during low-cost periods or favorable road conditions.*

Assumption 8. *The EV charging process is represented by an SOC-dependent nonlinear charging function. Vehicles may wait before charging when all chargers at a selected station are occupied.*

Assumption 9. *Charging costs differ between private and public charging stations. The charging decision of each vehicle is jointly affected by charging price, SOC level, charger availability, and subsequent route feasibility.*

2.3. Notation

To facilitate the formulation of the proposed electric refrigerated vehicle routing model, the main sets, parameters, and decision variables used in this study are summarized in Table 1.

Table 1. Notation Table.

Parameter	Description of Symbols
O	Distribution center
E	Set of electric vehicles, $k \in E$ denotes a vehicle
C	Set of customers, $i \in C$ denotes a customer
R	Set of private charging stations
U	Set of public charging stations
D	Set of all nodes, $D = \{O\} \cup C \cup R \cup U$
B	Maximum battery capacity
E^{d}_{ijk}	Driving energy consumption of vehicle k from node i to node j
$f_{ij}(t_1)$	Energy consumption rate from node i to j, depends on time period t_1 and traffic conditions
f_e	Energy consumption rate when vehicle is empty
v_{ij}	Vehicle travel speed
w_{ij}	Vehicle real-time load
α_1	Load sensitivity coefficient for energy consumption
β_1	Speed sensitivity coefficient for energy consumption
d_{ij}	Distance between nodes i and j, $i, j \in D$
e_0	Basic energy consumption rate under empty-load conditions
λ_1	Road gradient sensitivity coefficient for energy consumption
$\sin\theta_{ij}$	Road gradient angle of arc $i - j$
μ_1	Stop-and-go traffic conditions sensitivity coefficient for energy consumption
S_{ij}	Stop-and-go traffic intensity coefficient, which can be represented by congestion level, number of intersections, or stop–start frequency
δ_1	Ambient temperature sensitivity coefficient for energy consumption
T	Ambient temperature
T_0	Reference ambient temperature
a_1	Fixed cost per vehicle
c_1	Base electricity price
c_d	Travel distance cost per vehicle
c_2	Service fee
α	Electricity price fluctuation coefficient
t	Charging time
q^{e}_{i}	Charging amount of vehicle e at node i
ρ_i	Charging station type indicator, if $i \in R$, $\rho_i = 0$; if $i \in U$, $\rho_i = 1$
c_c	Charging price
ε_k	Energy consumption per unit distance for vehicle k (kWh/km)
ρ_k	$\rho_k \in (0, 1)$, proportion of public charging in vehicle k's route
t_k	Total refrigeration time required during operation for vehicle k
t^{d}_{k}	Refrigeration time during vehicle k's travel
t^{l}_{k}	Refrigeration time during vehicle k's unloading
t^{c}_{k}	Refrigeration time during vehicle k's charging
φ_k	Refrigeration power of vehicle k

Table 1. *Cont.*

Parameter	Description of Symbols
c_c^l	Refrigeration cost per unit time for vehicle k
p_t	Conversion efficiency of vehicle k
β_1	Loss coefficient during unloading
β_2	Loss coefficient during non-unloading
$t_i^{(n)}$	Non-unloading time for customer i
$t_i^{(u)}$	Unloading time for customer i
q_i	Demand of customer i
c_3	Unit cost of cargo loss
$[e_i, l_i]$	Service time window of customer i
c_4, c_5	Unit penalty cost for time window violation
δ_i^k	Arrival time of vehicle k at node i
μ_i^k	Departure time of vehicle k from node i
u_i^k	Battery level of vehicle k
$u_{j,in}^k$	Battery level of vehicle k upon arrival at charging station j
$u_{i,out}^k$	Battery level of vehicle k upon leaving node i after charging
z_{jh}^k	Selected feasible charging station h chosen by vehicle k after serving customer j
u_{ih}	Minimum energy required for vehicle to travel from node i to charging station h
s_i	Service start time of vehicle k
x_{ij}^k	0–1 variable, $x_{ij}^k = 0$ equals 1 if vehicle k travels from node i to j, otherwise 0
y_k	0–1 variable, indicates whether vehicle k is used
y_i^k	0–1 variable, indicates whether vehicle k charges at node i
$SOC_k(t)$	State of charge of vehicle k at time t
$E_k(t)$	Remaining battery energy of vehicle k at time t
P_s^{max}	Rated charging power of charging station s
$P_s(SOC_k(t))$	Effective charging power at charging station s under the current SOC of vehicle k
$\phi(SOC_k(t))$	SOC-dependent charging power coefficient
m_s	Number of chargers at charging station s
a_{sr}	Earliest available time of charger r at charging station s
t_{ks}^{arr}	Arrival time of vehicle k at charging station s
t_{ks}^{start}	Charging start time of vehicle k at charging station s
W_{ks}	Waiting time of vehicle k at charging station s
t_{ks}^{dep}	Departure time of vehicle k after charging at charging station s
T_{ks}^{chg}	Charging duration of vehicle k at charging station s
A	Set of directed road links
(i, j)	Directed link from node i to node j
d_{ij}	Length of link (i, j), consistent with the distance between nodes i and j
u_{ij}^0	Free-flow speed of link (i, j)
$u_{ij}(t)$	Time-dependent speed of link (i, j) at time t
q_{ij}^0	Basic traffic capacity of link (i, j)
$q_{ij}(t)$	Time-dependent traffic capacity of link (i, j) at time t
K_{ij}	Storage capacity of link (i, j)
ρ^{jam}	Jam density used to calculate link storage capacity
$\tau_{ij}^{ff}(t)$	Free-flow travel time on link (i, j) at time t
$h_{ij}(t)$	Minimum discharge headway of link (i, j)

2.4. Energy Consumption and Refrigeration Model

Drawing on existing modeling approaches for electric vehicle energy consumption, this study models the driving energy consumption of electric refrigerated vehicles as a function of travel distance, vehicle load, travel speed, road gradient, stop-and-go traffic conditions, and ambient temperature. Therefore, the relationship between energy consumption, vehicle load, speed, and distance is treated as part of the energy consumption function rather than as an independent assumption [45].

$$f_{ij}(t_1) = f_e(v_{ij}, t_1) \cdot \left(1 + \alpha_1 \cdot \frac{w_{ij}}{w_{max}}\right) \cdot \left(1 + \beta_1 \cdot \frac{v_{ij}^2}{v_{max}^2}\right) \tag{1}$$

According to the above formula, the vehicle's load directly affects battery consumption: a heavier load requires more energy to overcome inertia and friction, leading to higher power usage.

Vehicle speed also influences battery consumption: the closer the speed is to the maximum speed, the greater the incremental energy required.

Moreover, traffic conditions at different times of day impact vehicle speed, which in turn affects battery consumption. During peak hours, congestion reduces speed, resulting in relatively lower energy consumption; under off-peak or free-flow conditions, higher speeds can increase battery usage.

2.5. Nonlinear Charging and Charging Station Queuing Model

To address the limitation of the linear charging assumption, this study introduces an SOC-dependent nonlinear charging model. In practical EV charging, the charging power is not constant over the entire charging process. The charging speed is usually higher at low and medium SOC levels, while it gradually decreases when the battery approaches a high SOC range. Therefore, the effective charging power at charging station s is defined as follows:

$$P_s(SOC) = P_s^{max} \cdot \phi(SOC) \tag{2}$$

where P_s^{max} denotes the rated charging power of charging station s, and $\phi(SOC)$ is the SOC-dependent charging power coefficient. The piecewise function of $P_s(SOC)$ is defined as:

$$\phi(SOC) = \begin{cases} 1.0, 0 \le SOC < 0.60 \\ 1.0 - 2.0(SOC - 0.60), 0.60 \le SOC < 0.85 \\ 0.5 - 2.0(SOC - 0.85), 0.85 \le SOC \le 1.00 \end{cases} \tag{3}$$

Compared with the original linear charging formula, this formulation avoids systematically underestimating the charging time in high-SOC ranges. In this study, the rated charging powers of the depot, private charging stations, and public charging stations are set to 100 kW, 80 kW, and 60 kW, respectively.

In addition, to represent competition for limited charging resources, a shared-charger queuing mechanism is introduced. For charging station s, let m_s denote the number of chargers, and each charger maintains its earliest available time. When vehicle k arrives at station s at time t_{ks}^{arr}, its charging start time is determined by:

$$t_{ks}^{start} = \max\left(t_{ks}^{arr}, \min_{r=1,\ldots,m_s} a_{sr}\right) \tag{4}$$

where a_{sr} denotes the earliest available time of charger r at station s. The waiting time of vehicle k at station s is then calculated as:

$$W_{ks} = t_{ks}^{start} - t_{ks}^{arr} \tag{5}$$

The departure time after charging is given by:

$$t_{ks}^{dep} = t_{ks}^{start} + T_s^{chg}(SOC_a, SOC_b) \tag{6}$$

After the charging service is completed, the earliest available time of the corresponding charger is updated to t_{ks}^{dep}. This mechanism allows multiple vehicles in the same solution to share the charging station service state. The resulting queuing time is further transmitted to the calculation of time-window penalties, refrigeration cost, and subsequent route feasibility.

2.6. Link-Based Time-Dependent Travel Time and Congestion Propagation Model

To address the limitation of the global constant-speed assumption, this study introduces a link-based time-dependent travel time model. Since the Solomon benchmark provides only the coordinates of the depot, customers, and charging stations, but does not include real GIS road topology, a synthetic directed road network is constructed based on geometric proximity. Specifically, a k-nearest-neighbor graph is first generated for all nodes. In this study, k is set to 5. If the initial graph is disconnected, the nearest node pairs between different connected components are gradually connected until the entire graph becomes connected. Each undirected edge is then converted into two directed links with opposite directions. For each directed link (i, j), its length is denoted by d_{ij}, its free-flow speed by u_{ij}^0, its basic capacity by q_{ij}^0, and its storage capacity by K_{ij}. According to the comparison between the link length and the median link length of the whole network, each link is classified as either a branch road or a trunk road. The free-flow speeds of branch roads and trunk roads are set to 40 km/h and 60 km/h, respectively, and their corresponding basic capacities are set to 600 vehicles per hour (vph) and 900 vph.

To reflect peak-hour congestion, the free-flow speed and basic capacity of each link are reduced during peak periods:

$$u_{ij}(t) = \begin{cases} 0.75u_{ij}^0, \text{if t falls within peak periods,} \\ u_{ij}^0, \text{otherwise.} \end{cases} \tag{7}$$

$$q_{ij}(t) = \begin{cases} 0.65q_{ij}^0, \text{if t falls within peak periods,} \\ q_{ij}^0, \text{otherwise.} \end{cases} \tag{8}$$

The free-flow travel time of link (i, j) at time t is calculated as:

$$\tau_{ij}^{ff}(t) = \frac{60d_{ij}}{u_{ij}(t)} \tag{9}$$

Furthermore, to describe vehicle accumulation and spillback, each link is assigned a finite storage capacity:

$$K_{ij} = \rho^{jam} d_{ij} \tag{10}$$

$K_{ij} = \rho^{jam} d_{ij}$ $\left(\rho^{jam} = 18\right)$ veh/km denotes the jam density. If a vehicle is ready to enter link (i, j) but the current number of vehicles on this link has reached K_{ij}, the vehicle must wait upstream until the link becomes available. At the exit side, vehicles are discharged according to the link service rate $q_{ij}(t)$, and the minimum discharge headway is defined as:

$$h_{ij}(t) = \frac{60}{q_{ij}(t)} \tag{11}$$

Therefore, the actual exit time of a vehicle from a link is determined by the larger value between the free-flow exit time and the capacity-constrained discharge time. This design is equivalent to a finite-storage point-queue model, which can capture both time-dependent travel time and congestion propagation caused by multiple vehicles sharing the same road network.

It should be noted that the synthetic network is constructed because the Solomon benchmark does not provide real GIS road topology or observed traffic flow data. Therefore, the purpose of this network is to represent link-level time dependence and congestion propagation mechanisms rather than to reproduce a specific real-world road geometry.

2.7. Objective Function and Constraints

The objective function retains the original cost structure, including fixed vehicle cost, transportation cost, charging cost, refrigeration cost, cargo damage cost, and time-window penalty cost. However, the travel time, charging time, waiting time, and refrigeration duration are no longer calculated solely based on static distance and constant charging power. Instead, they are jointly determined by the SOC-dependent charging process, charging-station queuing status, and link-based time-dependent travel time. Charging waiting time and congestion delay are not counted as independent penalty terms; rather, they indirectly affect the total cost by extending vehicle operation time, increasing refrigeration costs, influencing time-window penalties, and altering subsequent route feasibility.

The fixed usage cost of EVs, which mainly includes vehicle purchase cost, fixed insurance, and basic maintenance fees, is proportional to the number of vehicles used, as expressed in Equation (12):

$$A_1 = \sum_{k \in E} a_1 y_k \tag{12}$$

The driving cost of EVs is proportional to the distance traveled, as shown in Equation (13):

$$A_2 = \sum_{k \in E} \sum_{i \in D} \sum_{j \in D} d_{ij} \cdot c_1 \cdot x_{ij}^k \tag{13}$$

The charging cost of EVs is defined as in Equation (14):

$$A_3 = \sum_{k \in E} \sum_{i \in R \cup U} y_i^k [c_1 \cdot (1 + \alpha \rho_i) + c_2 \rho_i] \cdot q_i^e \tag{14}$$

The cooling cost of EVs is expressed in Equation (15):

$$A_4 = \sum_{k \in E} \left(t_k^d + t_k^l\right) \cdot \varphi_k \cdot \left(c_c^l + p_t\right) + \sum_{k \in E} t_k^c \cdot \varphi_k \cdot \left(c_c^l + p_t\right) \tag{15}$$

The cargo damage cost is given by Equation (16):

$$A_5 = \sum_{k \in E} \sum_{i \in C} q_i \left[\left(1 - e^{-\beta_1 t_i^{(u)}}\right) + \left(1 - e^{-\beta_2 t_i^{(n)}}\right) \right] c_3 \tag{16}$$

The time window penalty cost is defined as in Equation (17):

$$A_6 = c_4 \sum_{i \in C} \max\left(0, e_i - \delta_i^k\right) + c_5 \sum_{i \in C} \max\left(0, \mu_i^k - l_i\right) \tag{17}$$

The overall objective function is thus formulated as:

$$\min A = (A_1 + A_2 + A_3 + A_4 + A_5 + A_6) \tag{18}$$

Constraints:

$$\sum_{k \in E} \sum_{j \in D, j \neq i} x_{ij}^k = 1, \forall i \in C \tag{19}$$

$$\sum_{i \in D, i \neq j} x_{ij}^k = \sum_{m \in D, m \neq j} x_{jm}^k, \forall j \in (C \cup R \cup U), \forall k \in E \tag{20}$$

$$\sum_{i\in C}\sum_{j\in D} x_{ij}^{k}\cdot q_i \leq Q_{max} y_k, \forall k \in E \tag{21}$$

$$\sum_{j\in D\backslash\{O\}} x_{Oj}^{k} = y_k, \sum_{i\in D\backslash\{O\}} x_{iO}^{k} = y_k, \forall k \in E \tag{22}$$

$$\sum_{h\in F} y_{jhk} = \rho_{jk},\ \forall j \in N, k \in K \tag{23}$$

$$x_{jhk} = y_{jhk},\ \forall j \in N, h \in F, k \in K \tag{24}$$

$$B_{jk} \geq E_{jhk} - M\left(1 - y_{jhk}\right),\ \forall j \in N, h \in F, k \in K \tag{25}$$

$$z_{jh}^{k} \leq \sum_{m\in D} x_{jm}^{k}, \sum_{h\in R\cup U} x_{jh}^{k} \leq M \sum_{h\in R\cup U} z_{jh}^{k} \tag{26}$$

$$u_{j,in}^{k} \geq u_{i,out}^{k} - u_{ij}^{k} - M\left(1 - x_{ij}^{k}\right) \tag{27}$$

$$u_{j,in}^{k} \leq u_{i,out}^{k} - u_{ij}^{k} + M\left(1 - x_{ij}^{k}\right) \tag{28}$$

$$u_{i,out}^{k} \geq \min e_{ih}, \forall i \in C, k \in E, h \in R \cup U \tag{29}$$

$$0 \leq u_{i,in}^{k} \leq B, 0 \leq u_{i,out}^{k} \leq B, \forall i \in D, k \in E \tag{30}$$

$$t_k = t_k^d + t_k^l + t_k^c, \forall k \in E \tag{31}$$

$$0 \leq u_i^k \leq B, \forall i \in D, \forall k \in E, u_O^k = B \tag{32}$$

$$\sum_{k\in E} x_{ij}^{k} \leq |H| - 1, \forall i, j \in D \tag{33}$$

$$s_i \geq \delta_i^k, \forall i \in C \tag{34}$$

$$s_i \geq e_i, E_i \geq e_i - \delta_i^k, L_i \geq s_i - l_i, E_i, L_i \geq 0, \forall i \in C \tag{35}$$

Constraint (19) ensures that each customer is served exactly once. Constraint (20) is the flow balance constraint. Constraint (21) is the vehicle capacity constraint, which ensures that the total customer demand carried by each vehicle on its route does not exceed the maximum vehicle load capacity. Constraint (22) ensures that each activated vehicle departs from the depot O and returns to the depot; vehicle k must depart from and return to the depot. Constraint (23) ensures that if vehicle k needs to visit a charging station after serving customer j, exactly one charging station is selected from the set of available public and private charging stations. Constraint (24) links the charging-station selection variable with the route decision variable, ensuring that if charging station hhh is selected, the corresponding route arc from customer j to charging station h must be generated. Constraint (25) guarantees that the vehicle has sufficient remaining battery to reach the selected charging station. Therefore, the charging station is not predetermined simply by distance; instead, it is selected jointly according to route feasibility and the total cost minimization objective. Constraint (26) further maintains the consistency between the customer-departure decision and the charging-station visiting decision. The first part defines the auxiliary variable z_{jh}^{k} according to whether vehicle k leaves customer node j. The second part restricts the generation of route arcs from customer j to charging stations, so that a vehicle can travel to a charging station only when the corresponding customer-departure decision is activated. This avoids infeasible route structures in which a charging-station arc is generated independently of the customer service sequence.Constraints (27) and (28) describe the battery propagation relationship along each selected route arc. When vehicle k travels from node i to node j, the battery level upon arriving at node j equals the battery level upon leaving node iii minus the energy consumption on arc (i,j). The big-M term relaxes this relationship when arc (i,j) is not selected. Constraint (29) ensures that after serving a customer, the vehicle has sufficient remaining battery either to continue to the next planned node or to reach the selected feasible charging station for recharging. This constraint prevents infeasible routes caused by battery depletion and maintains the energy feasibility of the route. Constraint (30) ensures that vehicle battery levels never drop below zero. Constraint (31) ensures that the refrigeration time of each vehicle covers the entire cold-chain delivery process, including traveling, customer unloading, and charging. In this study, temperature control is ensured at the route-optimization level by assuming that each electric refrigerated vehicle is equipped with a thermostatically controlled refrigeration unit. The refrigeration unit operates continuously during traveling, unloading, and charging. Therefore, the total refrigeration time of vehicle k is defined as the sum of traveling refrigeration time, unloading refrigeration time, and charging refrigeration time. A route is considered feasible only when the vehicle can complete the delivery process under continuous refrigerated operation while satisfying the battery-capacity and customer time-window constraints. The corresponding refrigeration cost and cargo damage cost are incorporated into the objective function to penalize routes with excessive transportation, unloading, or charging duration. Constraint (32) requires that at each node, vehicle battery levels are greater than or equal to zero and less than or equal to the maximum battery capacity B; vehicles depart the depot O fully charged. Constraint (33) is the subtour elimination constraint. Constraint (34) ensures that the vehicle service start time cannot be earlier than the arrival time. Constraint (35) allows for certain early arrivals and delays but requires paying the associated costs.

2.8. Improved Grey Wolf Algorithm

2.8.1. Greedy Insertion Algorithm for Initial Population Optimization

The initial population affects the search speed and direction of the algorithm in its early stages. Randomly generating the initial population can maintain diversity, but if the alpha and beta wolves generated randomly happen to fall into local optima, the search process may deviate from the direction of the global feasible optimum, ultimately resulting in infeasible solutions.

The improved Grey Wolf Algorithm enhances the selection mechanism for alpha and beta wolves to improve the quality of the initial population. Alpha and beta wolves with outstanding early performance are selected as the core of the initial population. First, the fitness of each wolf can be calculated as:

$$\mathrm{f}(\mathrm{X_i}) = \text{Objective Function Value of } \mathrm{X_i} \tag{36}$$

The top N wolves with the best fitness are selected as the initial population:

$$\mathrm{X_i} = \{\mathrm{X_1}, \mathrm{X_2}, \ldots, \mathrm{X_N}\} \tag{37}$$

where $\mathrm{X_1}, \mathrm{X_2} \ldots \mathrm{X_N}$ are high-quality alpha and beta wolves in the initial population.

The selection of alpha and beta wolves considers not only their fitness but also their leadership ability within the pack. Both criteria are used to choose the initial population, expressed as:

$$X_{best} = argminf(X_i),\ 1 \le i \le N \tag{38}$$

The position update formula for the wolf pack is:

$$\mathrm{X_i^{(t+1)}} = \mathrm{X_i^t} + \mathrm{r_1}\left(\mathrm{X_A} - \mathrm{X_i^{(t)}}\right) + \mathrm{r_2}\left(\mathrm{X_B} - \mathrm{X_i^{(t)}}\right) \tag{39}$$

2.8.2. Dynamic Proportional Weight Position Update Strategy

In the original Grey Wolf Algorithm, the ω wolves update their positions by following the α, β, and δ wolves as:

$$\begin{cases} X_1 = X_\alpha - A_1 D_\alpha \\ X_2 = X_\beta - A_2 D_\beta \\ X_3 = X_\delta - A_3 D_\delta \end{cases} \tag{40}$$

According to the dynamic proportional weight strategy, the weight ratios of the three wolves for the ω wolves are:

$$\begin{aligned} \omega_1 &= \frac{|X_1|}{|X_1| + |X_2| + |X_3|} \\ \omega_2 &= \frac{|X_2|}{|X_1| + |X_2| + |X_3|} \\ \omega_3 &= \frac{|X_3|}{|X_1| + |X_2| + |X_3|} \end{aligned} \tag{41}$$

Here, $\omega_1, \omega_2, \omega_3$ represent the positional influence weights of α, β, and δ wolves on the ω wolves. After introducing the dynamic proportional weights, the final position of ω wolves is:

$$X_{(t+1)} = \frac{\omega_1 X_1 + \omega_2 X_2 + \omega_3 X_3}{3} \tag{42}$$

The "destroy–repair" operator performs local optimization on the positions of the alpha and beta wolves, enhancing their search capability. The destroy operator expands the search space and prevents premature convergence by randomly perturbing the current solution. In the destroy phase, the current solution X_i is disturbed to break its local structure, where ΔX_i is the perturbation variable, which can be random or a local modification of the search space, expressed as:

$$X_i^d = X_i + r_1 \cdot \Delta X_i \tag{43}$$

The repair operator reconstructs the disturbed solution using a greedy criterion, ensuring feasibility while improving solution quality. Let Ω denote the set of all feasible solutions. Then:

$$X_i^r = \mathrm{agrminf}(X_i), X_i \in \Omega \tag{44}$$

After each iteration, dynamic search adjusts the weights to optimize the path search process. $\omega(t)$ is the dynamic weight function, which is gradually adjusted with increasing iterations to improve the search for the optimal path. The position update formula for alpha and beta wolves is:

$$X_i^{(t+1)} = X_i^t + \omega(t) \cdot r_1 \left(X_A - X_i^{(t)} \right) + \omega(t) \cdot r_2 \left(X_B - X_i^{(t)} \right) \tag{45}$$

The local optimization of the destroy–repair operator improves the search mechanism of the Grey Wolf Algorithm, enabling effective convergence to the optimal solution of the objective function. That is, let X_O denote the optimal solution position:

$$C(X_O) = \mathrm{minf}(X_O) \tag{46}$$

2.8.3. Destroy–Repair Operator

To provide a clearer description of the local search procedure, the destroy–repair operator is formalized as follows. The operator first destroys part of the current route structure by removing a subset of customer nodes, and then repairs the solution by reinserting these nodes into feasible positions. During the repair process, feasibility with respect to vehicle capacity, customer time windows, battery level, and charging-station accessibility is checked sequentially. If a candidate insertion violates the battery constraint, a feasible charging station is inserted before the infeasible arc. If no feasible repair can be found, the corresponding solution is penalized and excluded from the elite population.

To further clarify the implementation procedure and improve reproducibility, the pseudo-code of the destroy–repair operator is summarized in Table 2.

Table 2. Pseudo-code of the destroy–repair operator.

Step	Procedure
Input	Current solution (X), customer set (N), charging station set (F), removal ratio (r).
Output	Repaired solution (X′).
1	Decode (X) into vehicle routes.
2	Select (r%) of customer nodes from the current routes according to a random or relatedness-based removal rule.
3	Remove the selected customers from the routes and store them in set (R).
4	Remove redundant charging-station nodes if they are no longer needed.
5	For each removed customer (j ∈ R), enumerate all possible insertion positions in all routes.
6	For each candidate insertion position, check vehicle capacity feasibility, customer time-window feasibility, and battery feasibility before and after insertion.
7	If the battery constraint is violated, insert a feasible charging station before the infeasible arc and update the battery level and charging time.
8	Calculate the incremental total cost of each feasible insertion position.
9	Insert customer (j) into the feasible position with the minimum incremental cost.
10	If all customers are inserted and all constraints are satisfied, return the repaired solution (X′).
11	Otherwise, assign a penalty value to (X′) and reject it from the elite population.

2.8.4. Adaptive Position Update Mechanism

In the standard Grey Wolf Optimizer, if the difference between the α wolf and the β wolf is excessively large, the population may move in dispersed directions, leading to slow convergence and low search efficiency. Conversely, if the difference between the leading wolves becomes too small at an early stage, the population may converge prematurely to a local optimum. To address this issue, an adaptive update mechanism is introduced to dynamically adjust the disturbance intensity and balance global exploration with local exploitation.

The difference between the α wolf and the β wolf is used to measure the population dispersion. A larger difference indicates that the population is still widely distributed, and thus a stronger disturbance is introduced to enhance global exploration. A smaller difference indicates that the population has entered a promising search region, and the disturbance is reduced to strengthen local exploitation.

The adaptive disturbance coefficient is defined as:

$$\lambda_t = \lambda_{min} + (\lambda_{max} - \lambda_{min}) \frac{D^t_{\alpha\beta}}{D_{max}} \left(1 - \frac{t}{T_{max}}\right) \quad (47)$$

where $D^t_{\alpha\beta}$ denotes the difference between the α wolf and the β wolf at iteration t, D_{max} is the maximum difference observed in the population, t is the current iteration, and T_{max} is the maximum number of iterations. As the iteration proceeds, the disturbance intensity gradually decreases, which helps the algorithm shift from global exploration to local exploitation.

To further clarify the implementation procedure of the adaptive update mechanism, its pseudo-code is presented in Table 3.

Table 3. Pseudo-code of the adaptive update mechanism of IGWO.

Step	Procedure
Input	Population X_t, alpha wolf X_α, beta wolf X_β, delta wol X_δ, current iteration t, maximum iteration T_{max}.
Output	Updated populationX_{t+1}.
1	Calculate the difference $D_{\alpha\beta}$ between X_α and X_β.
2	Compute the adaptive disturbance coefficient λ_t
3	For each wolf X_i in the population, update X_i according to the weighted guidance of X_α, X_β, and X_δ.
4	Add adaptive disturbance controlled by λ_t.
5	Decode the updated position into a route solution.
6	Apply the destroy–repair operator to restore feasibility.
7	Evaluate the fitness value of the repaired solution.
8	Update X_α, X_β, and X_δ according to the fitness ranking.
9	Preserve the best-so-far solution using an elitist strategy.
10	Return the updated population X_{t+1}.

2.8.5. Local Optimization Operation

In the Grey Wolf Algorithm, if the difference between the solutions of the alpha and beta wolves is large, the wolves may converge slowly and move in dispersed directions during the convergence process, which reduces the global search efficiency and convergence speed of the algorithm. To avoid this situation, an adaptive position update strategy for the ω wolves is introduced. The improved Grey Wolf Algorithm not only enhances the coordination of the wolf pack but also improves the stability and robustness of the algorithm in solving the cold chain logistics routing optimization problem. The position of the wolf pack is adjusted according to the dynamic difference between the alpha and beta wolves. Let Δ denote the difference measure between the alpha and beta wolves. The difference measure function is defined as:

$$\Delta = \frac{1}{N}\sum_{i=1}^{N}|X_A - X_B| \quad (48)$$

According to the difference measure, the strategy for dynamically adjusting the position update of the wolf pack is as follows:

When Δ is large, the exploration ability of the wolf pack is enhanced by increasing the disturbance in the position update:

$$X_i^{(t+1)} = X_i^t + \omega(t)\cdot r_1\left(X_A - X_i^{(t)}\right) + \omega(t)\cdot r_2\left(X_B - X_i^{(t)}\right) \quad (49)$$

When Δ is small, the exploitation ability of the wolf pack is strengthened and the disturbance is reduced:

$$X_i^{(t+1)} = X_i^t + \omega(t)\cdot r_1\left(X_A - X_i^{(t)}\right) \quad (50)$$

The adaptive update mechanism adjusts the search direction according to the distribution of the alpha and beta wolf solutions. When the difference between them is large, ordinary wolves increase the disturbance appropriately during the update process to avoid falling into local optima in the early stage. When the two become similar, unnecessary disturbances are reduced, guiding the wolf pack to converge rapidly to the optimal solution.

To more clearly illustrate the operational logic of the adaptive update mechanism, the overall procedure is presented in Figure 1.

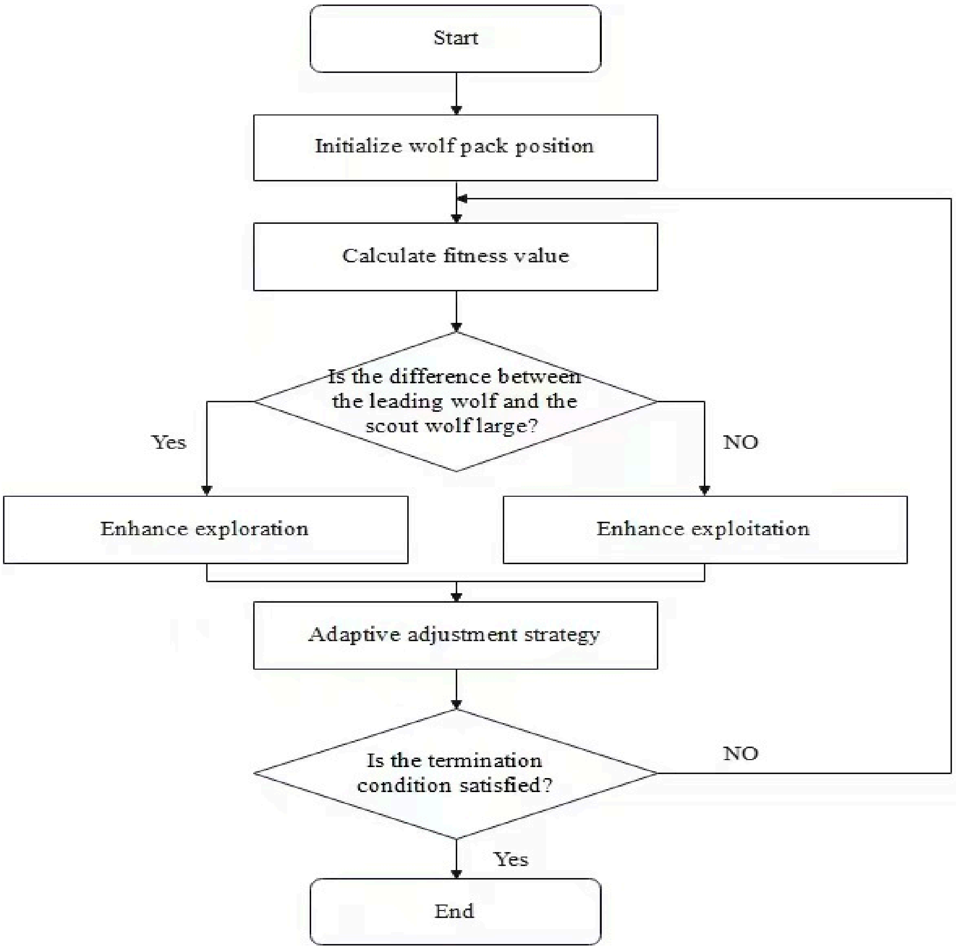

Figure 1. Operation Flowchart.

3. Results

This paper conducts numerical experiments based on the Solomon standard dataset C201 as the basic test instance. The original Solomon customer and depot data, including coordinates, demands, time windows, and service times, were retained unchanged; only six public charging stations and six private charging stations were added within the distribution area to adapt the instance to the electric vehicle cold-chain distribution scenario and support charging-related routing decisions. Specifically, the customer node coordinates were used as input data, and K-means clustering was applied to generate representative charging station locations. The number of clusters was set to 12, corresponding to 12 charging stations, and a fixed random seed was used during the clustering process to ensure the reproducibility of the experimental results.

3.1. Experimental Setup

The original Solomon C201 dataset is used as the basic benchmark instance in this study. The original customer and depot data, including coordinates, demands, time windows, and service times, are retained unchanged. The customer nodes and the additionally introduced charging-station nodes used in the experiment are summarized in Table 4.

Table 4. Solomon Dataset.

Node	Coordinate/km	Demand/kg	Time Window	Service Time/min	Node	Coordinate/km	Demand/kg	Time Window	Service Time/min
0	(40, 50)	--	--	--	57	(38, 15)	40	[1725, 1885]	90
1	(52, 75)	10	[311, 471]	90	58	(38, 5)	30	[1442, 1602]	90
2	(45, 70)	30	[213, 373]	90	59	(38, 10)	10	[1630, 1790]	90
3	(62, 69)	10	[1167, 1327]	90	60	(35, 5)	20	[1535, 1695]	90
4	(60, 66)	10	[1261, 1421]	90	61	(50, 30)	10	[401, 561]	90
5	(42, 65)	10	[25, 185]	90	62	(50, 35)	20	[120, 280]	90
6	(16, 42)	20	[497, 657]	90	63	(50, 40)	50	[25, 185]	90
7	(58, 70)	20	[1073, 1233]	90	64	(48, 30)	10	[493, 653]	90
8	(34, 60)	20	[2887, 3047]	90	65	(44, 25)	10	[871, 1031]	90
9	(28, 70)	10	[2601, 2761]	90	66	(47, 35)	10	[588, 748]	90
10	(35, 66)	10	[2791, 2951]	90	67	(47, 40)	10	[12, 172]	90
11	(35, 69)	10	[2698, 2858]	90	68	(42, 30)	10	[776, 936]	90
12	(25, 85)	20	[2119, 2279]	90	69	(45, 35)	10	[680, 840]	90
13	(22, 75)	30	[2405, 2565]	90	70	(95, 30)	30	[2321, 2481]	90
14	(22, 85)	10	[2026, 2186]	90	71	(95, 35)	20	[2226, 2386]	90
15	(20, 80)	40	[2216, 2376]	90	72	(53, 30)	10	[308, 468]	90
16	(20, 85)	40	[1934, 2094]	90	73	(92, 30)	10	[2414, 2574]	90
17	(18, 75)	20	[2311, 2471]	90	74	(53, 35)	50	[213, 373]	90
18	(15, 75)	20	[1742, 1902]	90	75	(45, 65)	20	[118, 278]	90
19	(15, 80)	10	[1837, 1997]	90	76	(90, 35)	10	[2131, 2291]	90
20	(30, 50)	10	[10, 170]	90	77	(72, 45)	10	[2900, 3060]	90
21	(30, 56)	20	[2983, 3143]	90	78	(78, 40)	20	[2802, 2962]	90
22	(28, 52)	20	[22, 182]	90	79	(87, 30)	10	[2608, 2768]	90
23	(14, 66)	10	[1643, 1803]	90	80	(85, 25)	10	[2513, 2673]	90
24	(25, 50)	10	[116, 276]	90	81	(85, 35)	30	[2703, 2863]	90
25	(22, 66)	40	[2504, 2664]	90	82	(75, 55)	20	[1925, 2085]	90
26	(8, 62)	10	[1545, 1705]	90	83	(72, 55)	10	[1832, 1992]	90
27	(23, 52)	10	[209, 369]	90	84	(70, 58)	20	[1641, 1801]	90
28	(4, 55)	20	[1447, 1607]	90	85	(86, 46)	30	[2029, 2189]	90
29	(20, 50)	10	[398, 558]	90	86	(66, 55)	10	[1736, 1896]	90
30	(20, 55)	10	[303, 463]	90	87	(64, 46)	20	[3097, 3257]	90
31	(10, 35)	20	[781, 941]	90	88	(65, 60)	30	[1546, 1706]	90
32	(10, 40)	30	[593, 753]	90	89	(56, 64)	10	[1355, 1515]	90
33	(8, 40)	40	[685, 845]	90	90	(60, 55)	10	[3119, 3279]	90
34	(8, 45)	20	[1346, 1506]	90	91	(60, 60)	10	[1451, 1611]	90
35	(5, 35)	10	[876, 1036]	90	92	(67, 85)	20	[694, 854]	90
36	(5, 45)	10	[1253, 1413]	90	93	(42, 58)	40	[8, 168]	90
37	(2, 40)	20	[971, 1131]	90	94	(65, 82)	10	[788, 948]	90
38	(0, 40)	30	[1063, 1223]	90	95	(62, 80)	30	[881, 1041]	90
39	(0, 45)	20	[1158, 1318]	90	96	(62, 40)	10	[3001, 3161]	90
40	(36, 18)	10	[1819, 1979]	90	97	(60, 85)	30	[597, 757]	90
41	(35, 32)	10	[2758, 2918]	90	98	(58, 75)	20	[978, 1138]	90
42	(33, 32)	20	[2666, 2826]	90	99	(55, 80)	10	[407, 561]	90
43	(33, 35)	10	[2573, 2733]	90	100	(55, 85)	20	[502, 662]	90
44	(32, 20)	10	[1913, 2073]	90	1000	(49, 34)	--	--	--
45	(30, 30)	10	[2105, 2265]	90	1001	(18, 66)	--	--	--
46	(34, 25)	30	[2009, 2169]	90	1002	(67, 54)	--	--	--
47	(30, 35)	10	[2480, 2640]	90	1003	(6, 42)	--	--	--
48	(36, 40)	10	[2856, 3016]	90	1004	(39, 12)	--	--	--
49	(48, 20)	10	[967, 1127]	90	1005	(88, 34)	--	--	--
50	(26, 32)	10	[2292, 2452]	90	1006	(61, 83)	--	--	--
51	(25, 30)	10	[2200, 2360]	90	1007	(40, 65)	--	--	--
52	(25, 35)	10	[2385, 2545]	90	1008	(25, 52)	--	--	--
53	(44, 5)	20	[1256, 1416]	90	1009	(20, 80)	--	--	--
54	(42, 10)	40	[1160, 1320]	90	1010	(58, 70)	--	--	--
55	(42, 15)	10	[1065, 1225]	90	1011	(31, 33)	--	--	--
56	(40, 5)	30	[1350, 1510]						

Note: Node 0 represents the distribution center; nodes 1–100 represent customer locations; nodes 1006–1011 represent public charging stations; and nodes 1000–1005 represent private charging stations.

To simulate actual electric refrigerated vehicle operations, key vehicle-related parameters are specified in the numerical experiments, including battery capacity, vehicle maximum load, distance cost, electricity price, refrigeration power, refrigeration cost, cargo loss cost, time-window penalty coefficients, energy consumption parameters, charging power, and maximum driving range. These vehicle-related parameters are shown in Table 5.

Table 5. Vehicle-Related Parameters.

Symbol	Description	Units	Value
B	Battery Capacity	kWh	60
ω_{max}	Vehicle Maximum Load	kg	200
c_d	Distance Cost	CNY/km	0.8
c_1	Base Electricity Price	CNY/kWh	0.6
c_2	Service Fee	CNY/kWh	0.3
α	Electricity Price Fluctuation Coefficient	--	0.4
φ_k	Refrigeration Power	kw	2.0
c_c^l	Refrigeration Cost	CNY/h	0.4
p_t	Conversion Efficiency	--	0.9
c_4	Early Arrival Penalty	CNY/min	2.0
c_5	Late Arrival Penalty	CNY/min	4.0
c_3	Cargo Loss Cost	CNY/kg	8.0
β_1	Unloading Loss Coefficient	--	0.02
β_2	Non-Unloading Loss Coefficient	--	0.002
f_e	Base Energy Consumption	kWh/km	0.4
α_1	Weight Sensitivity	kWh/km·kg	0.05
β_1	Speed Sensitivity	kWh/km·(km/h)	0.1
v_{max}	Maximum Speed	km/h	80
p_c	Charging Power	kw	60
R_{max}	Maximum Driving Range	km	120

This paper adopts numerical experiments for analysis. The Solomon standard dataset C201 is used as the basic test instance. To adapt it to the electric vehicle cold chain distribution scenario, six public charging stations and six private charging stations are added within the distribution area, with their coordinates uniformly distributed across the service region.

For the nonlinear charging and queuing model, the rated charging powers of the depot, private charging stations, and public charging stations are set to 100 kW, 80 kW, and 60 kW, respectively. These settings are used to distinguish the service capability of different charging resources and to reflect possible queuing effects under limited charger availability.

For the link-based time-dependent travel time model, a synthetic directed road network is generated using a k-nearest-neighbor graph with k = 5. Branch roads and trunk roads are assigned free-flow speeds of 40 km/h and 60 km/h, respectively, with corresponding basic capacities of 600 veh/h and 900 veh/h. During peak periods, the link free-flow speed and link capacity are reduced by factors of 0.75 and 0.65, respectively. The jam density used to calculate finite link storage capacity is set to 18 veh/km.

3.2. Algorithm Performance Comparson

To further verify the proposed algorithm, GA, GWO, ALNS, and IGWO are compared for solution quality. Each algorithm was run four times on each benchmark instance. Table 6 reports the mean objective value and sample standard deviation.

Table 6. Optimization Results under Different Algorithms.

Case	GA	GWO	ALNS	IGWO
	Mean ± SD	Mean ± SD	Mean ± SD	Mean ± SD
C201	3620.98 ± 335.82	3410.19 ± 253.50	4939.88 ± 877.69	3331.64 ± 296.78
C202	3064.65 ± 188.50	3098.70 ± 272.07	3753.63 ± 626.79	2564.67 ± 310.55
C203	2575.83 ± 171.15	2767.02 ± 248.19	2998.23 ± 477.64	2494.55 ± 244.53
C204	2108.85 ± 81.53	2141.13 ± 175.31	2163.66 ± 201.90	2087.96 ± 121.19
C205	2891.42 ± 113.79	3032.75 ± 278.75	4609.67 ± 464.67	2958.00 ± 35.03
C206	2595.87 ± 238.44	2872.39 ± 163.36	3933.88 ± 667.19	2452.75 ± 213.65
C207	2753.23 ± 90.80	2716.25 ± 529.10	3687.86 ± 750.05	2747.50 ± 135.51
C208	2595.55 ± 127.92	2690.62 ± 120.43	3623.34 ± 859.52	2545.01 ± 136.70

Table 6 shows that IGWO achieves the best mean objective value in six of eight C-type Solomon instances. This suggests IGWO often outperforms GA, GWO, and ALNS. In several cases, IGWO has small standard deviations, indicating robust performance and stable solution quality.

Although GA achieves the lowest mean objective value in C205 and GWO performs slightly better in C207, the overall comparative results demonstrate the competitive performance of IGWO across different benchmark instances. Compared with GA and standard GWO, IGWO benefits from the high-quality initial population selection mechanism, the destroy–repair operator, and the adaptive position update strategy, which help balance global exploration and local exploitation. Compared with ALNS, IGWO also shows better average performance in most tested instances, indicating that the proposed algorithm is effective for solving the electric cold-chain vehicle routing problem under mixed public–private charging conditions.

Figure 2 compares the mean objective values of GA, GWO, ALNS, and IGWO over four independent runs on the C201–C208 benchmark instances. The height of each bar represents the mean objective value, while the error bar indicates the sample standard deviation. Since the objective of the model is to minimize the total cost, a lower bar indicates better solution quality, and a shorter error bar indicates more stable performance.

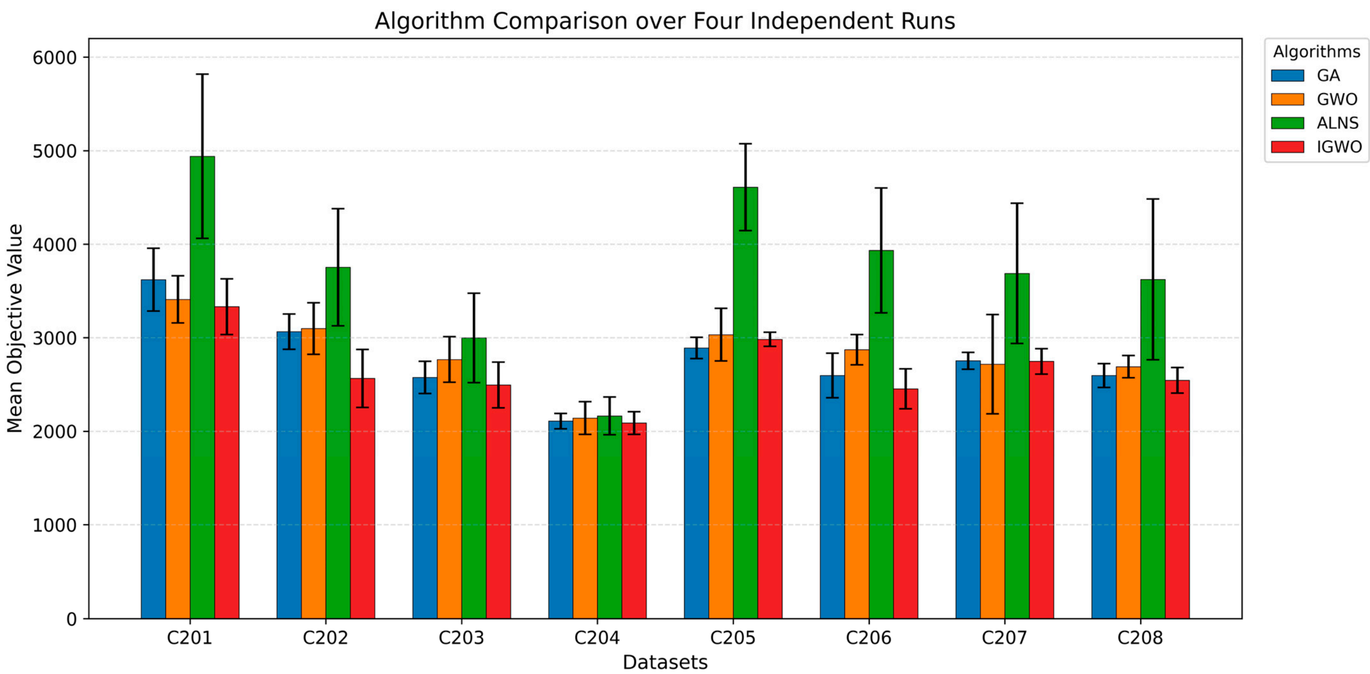

Figure 2. Algorithm Comparison Based on Mean Objective Values and Standard Deviations.

As shown in the figure, IGWO achieves the lowest mean objective value in most benchmark instances, including C201, C202, C203, C204, C206, and C208. This indicates that the proposed IGWO generally provides better solution quality than GA, GWO, and ALNS under repeated runs. Although GA performs slightly better in C205 and GWO performs slightly better in C207, IGWO still maintains competitive performance across all tested cases.

The error bars further show the robustness of different algorithms. ALNS exhibits relatively large fluctuations in several instances, such as C201, C206, C207, and C208, indicating that its performance is less stable under the current experimental setting. By contrast, IGWO generally maintains relatively small standard deviations while achieving lower mean objective values. This suggests that the proposed high-quality initial population selection mechanism, destroy–repair operator, and adaptive position update strategy can improve both the solution quality and robustness of the standard GWO.

Overall, Figure 2 demonstrates that IGWO achieves a better balance between optimization performance and solution stability for the electric cold-chain vehicle routing problem under the mixed public–private charging mode.

3.3. Route and Cost Comparson

The modified Solomon standard dataset C201 is used, with the number of vehicles set to ten. The experiment is conducted four times, and the optimal route is obtained. The optimal route is shown in the following figure, and the specific optimization results are presented in Figure 3. The delivery information of each vehicle is shown in Table 7.

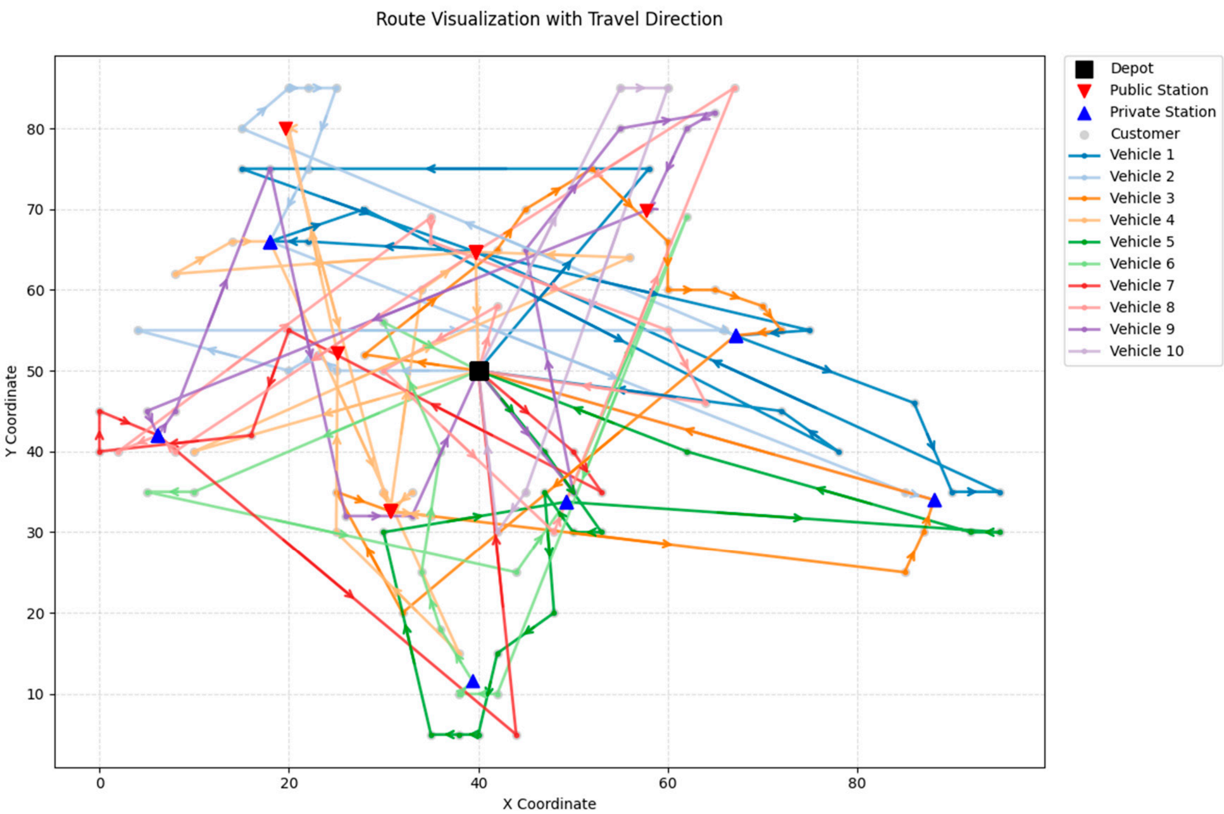

Figure 3. Route Visualization with Travel Direction.

Table 7. Delivery Information of Each Electric Vehicle.

No.	Delivery Routes
1	0→68→37→54→1005→53→40→42→41→78→77→87→0
2	0→32→33→35→7→86→84→1002→82→70→80→96→0
3	0→2→30→39→34→36→1001→57→52→25→10→1007→48→1009→0
4	0→20→22→27→61→49→56→59→1009→26→1001→44→46→1002→13→9→90→0
5	0→64→100→97→92→1002→38→18→23→1001→14→47→1009→79→1006→81→0
6	0→1→99→94→95→98→1003→55→58→60→45→51→50→43→0
7	0→93→5→75→74→3→4→89→8→0
8	0→63→66→69→65→91→88→83→85→76→1006→71→73→0
9	0→67→24→62→72→29→1008→6→1004→31→19→16→15→11→0
10	0→28→12→17→21→0

Figure 3 shows the optimized electric vehicle routing map under the mixed public–private charging mode. The black square represents the distribution center, the grey points represent customer nodes, the red triangles represent public charging stations, and the blue triangles represent private charging stations. Different colored lines indicate the delivery routes of different vehicles. As shown in the figure, all vehicles depart from the distribution center and return to the depot after completing their delivery tasks, forming closed delivery routes.

The routing results show that the proposed model can coordinate customer service, vehicle battery constraints, and charging station selection within the same optimization framework. When the remaining battery level is insufficient to support subsequent customer visits or the return trip to the depot, vehicles are guided to nearby public or private charging stations for energy replenishment. This indicates that the model can dynamically incorporate charging decisions into route planning rather than treating charging as a separate process.

The delivery cost analysis under different models for each route is shown in Table 8.

Table 8. Analysis of Delivery Costs under Different Models.

Cost Types	Public Charging Stations	Private Charging Stations	Mixed Public–Private Charging Stations
Fixed Cost	1200.00	1200.00	1200.00
Travel Cost	2655.94	2141.94	1913.33
Charging Cost	1136.13	571.88	450.78
Time Window Penalty Cost	763.98	751.60	828.53
Cargo Loss Cost	331.12	329.23	323.84
Refrigeration Cost	34.82	30.01	27.92
Total Cost	6121.99	5024.66	4744.40

3.4. Sensitivity Analysis

The electric vehicle routing problem studied in this paper involves the selection of public and private charging stations. When some parameters change, the distribution routes may show different optimization results. In this section, sensitivity analysis is conducted to discuss the impact of changes in certain parameters on the optimization results, providing reference value for the green and low-carbon transformation of cold chain distribution scenarios.

Since the sensitivity analysis is designed to evaluate the influence of model parameters rather than to conduct another full algorithm ranking, only GA, GWO, and IGWO are reported in this section. ALNS has already been included as a benchmark algorithm in the algorithm performance comparison section. The sensitivity analysis focuses on whether the proposed IGWO shows consistent parameter-response patterns under changes in battery capacity and energy efficiency.

3.4.1. On-Board Battery Capacity

The driving range of electric vehicles is limited by battery capacity. To meet different application scenarios, manufacturers also produce batteries with different capacities for the same type of vehicle. Considering this situation, based on the research framework, the battery capacity is adjusted to 60 kWh, 80 kWh, 90 kWh, 100 kWh, 110 kWh, 120 kWh, and 130 kWh. The charging amount, charging frequency, and total route cost obtained by the GA, GWO, and IGWO under different battery capacities are compared. The detailed comparison results are shown in Figures 4 and 5. In addition, when the battery capacity increases to 130 kWh, regardless of the charging mode adopted, vehicles can complete pickup and delivery tasks without recharging.

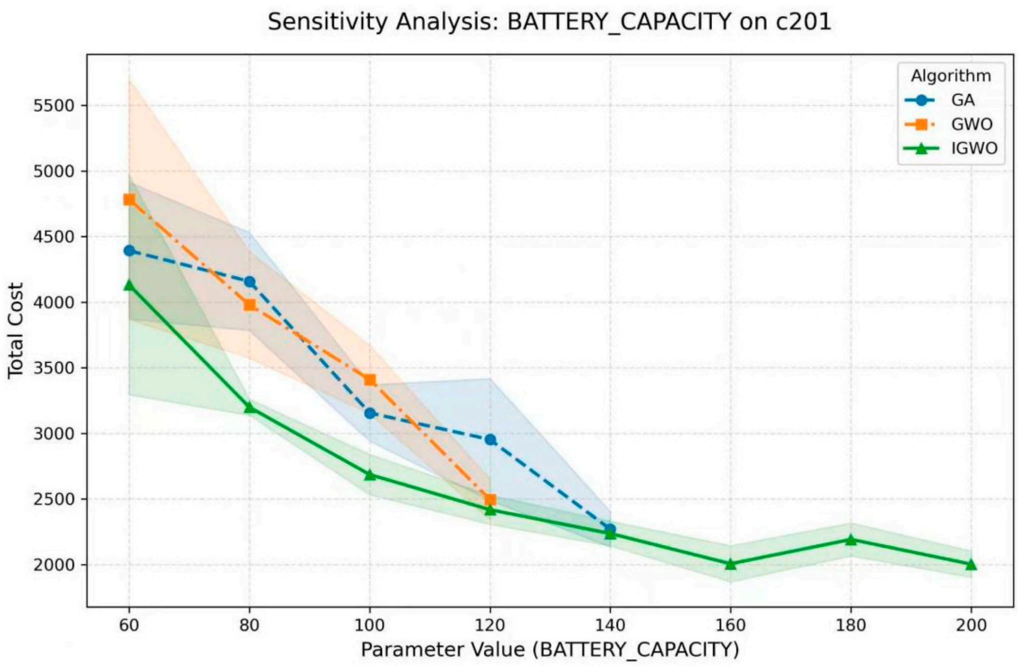

Figure 4. Trends of Total Cost and Cost Reduction Rate.

The shaded areas indicate the variability of the results obtained from repeated independent runs. Specifically, they represent the mean ± standard deviation range for each algorithm under each battery-capacity setting.

Figure 4 shows the impact of battery capacity on the total distribution cost under different algorithms. Overall, as battery capacity increases, the total cost shows a clear downward trend. This is mainly because a larger battery capacity extends the driving range of electric refrigerated vehicles, reduces the need for intermediate charging, and decreases charging-related detours and waiting time. When the battery capacity increases from 60 kWh to 120 kWh, the total cost decreases significantly, indicating that battery capacity is an important factor affecting the economic performance of electric cold-chain delivery. However, after the battery capacity reaches a relatively high level, the cost reduction becomes less obvious, suggesting that the marginal benefit of further increasing battery capacity gradually weakens.

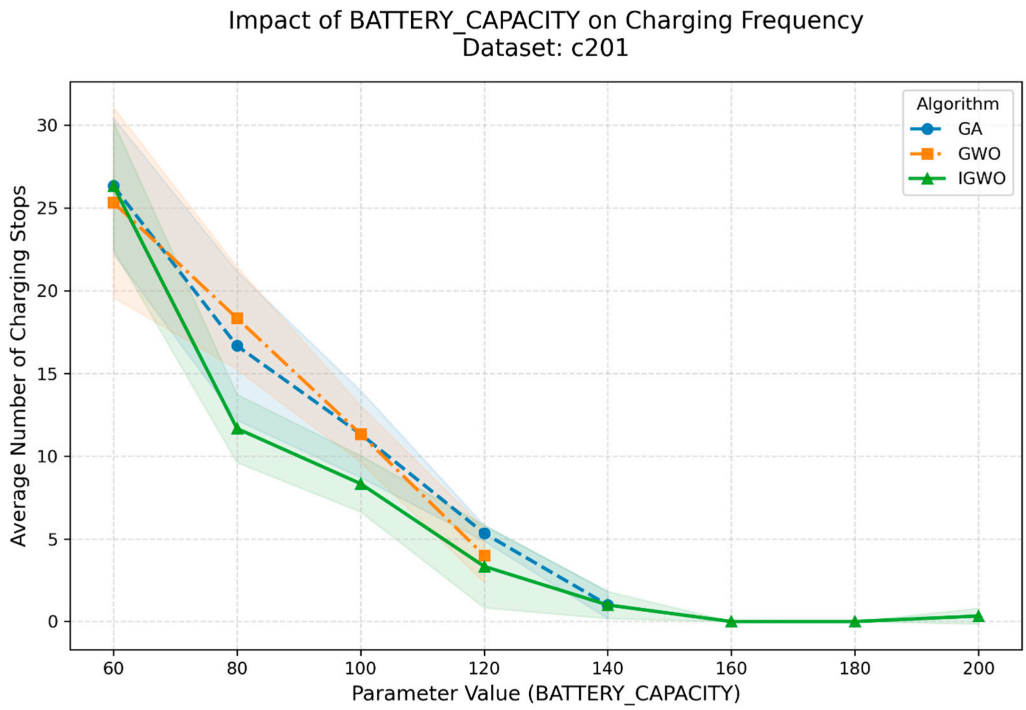

Figure 5. Trends of Charging Amount and Number of Charging Events.

Among the three algorithms, IGWO generally obtains lower total costs than GA and GWO under most battery capacity settings. This indicates that the proposed IGWO can better coordinate battery capacity, route planning, and charging decisions. In particular, under lower battery capacity conditions, vehicles face stronger energy constraints and need more frequent charging decisions. In this case, the advantage of IGWO is more obvious because its improved search mechanism can better avoid unnecessary detours and reduce infeasible or high-cost routing schemes.

Figure 5 further illustrates the influence of battery capacity on the average number of charging events. The number of charging events decreases rapidly as battery capacity increases. When the battery capacity is relatively low, such as 60 kWh or 80 kWh, vehicles need to visit charging stations more frequently to maintain route feasibility. As the battery capacity increases to 120 kWh or above, the number of charging events becomes very small, and in some cases, vehicles can complete their delivery tasks without en-route charging. This result confirms that increasing battery capacity can effectively reduce dependence on charging stations.

Overall, Figures 4 and 5 indicate that battery capacity has a significant influence on both total cost and charging behavior. A larger battery capacity can reduce charging frequency and improve route flexibility, thereby lowering the overall distribution cost. However, the marginal cost reduction gradually decreases when the battery capacity becomes sufficiently large. Therefore, for electric cold-chain logistics enterprises, battery capacity selection should consider not only driving range but also vehicle purchase cost, charging infrastructure conditions, and actual delivery demand.

3.4.2. Energy Conversion Coefficient

Due to the current technological limitations of battery systems, regardless of the medium used in electric vehicle batteries, the discharge performance of batteries is affected by external environmental factors such as weather. As a result, vehicles may consume more electricity when traveling the same distance under harsh environmental conditions. In this paper, the energy conversion coefficient θ is used to describe the relationship of electricity consumption for electric vehicles. A larger value of θ indicates that more electricity is required to travel the same distance. By adjusting the value of θ, the differences in route optimization results for electric vehicles under different environmental conditions are analyzed. In this section, the energy conversion coefficient is set to 1.05θ, 1.10θ, 1.15θ, 1.20θ, 1.25θ, 1.30θ. The comparison of total costs is shown in the following figure. As illustrated in the figure, with the continuous increase the energy coefficient, the total cost also increases continuously.

Figure 6 shows the influence of the energy conversion coefficient on the total distribution cost. As the energy conversion coefficient increases from 1.05 to 1.30, the total cost of all three algorithms shows an increasing trend. This is because a larger coefficient indicates higher electricity consumption for the same travel distance and load condition, which increases charging demand and charging-related costs. The shaded areas indicate the variability of the results obtained from repeated independent runs. Specifically, they represent the mean ± standard deviation range for each algorithm under each battery-capacity setting.

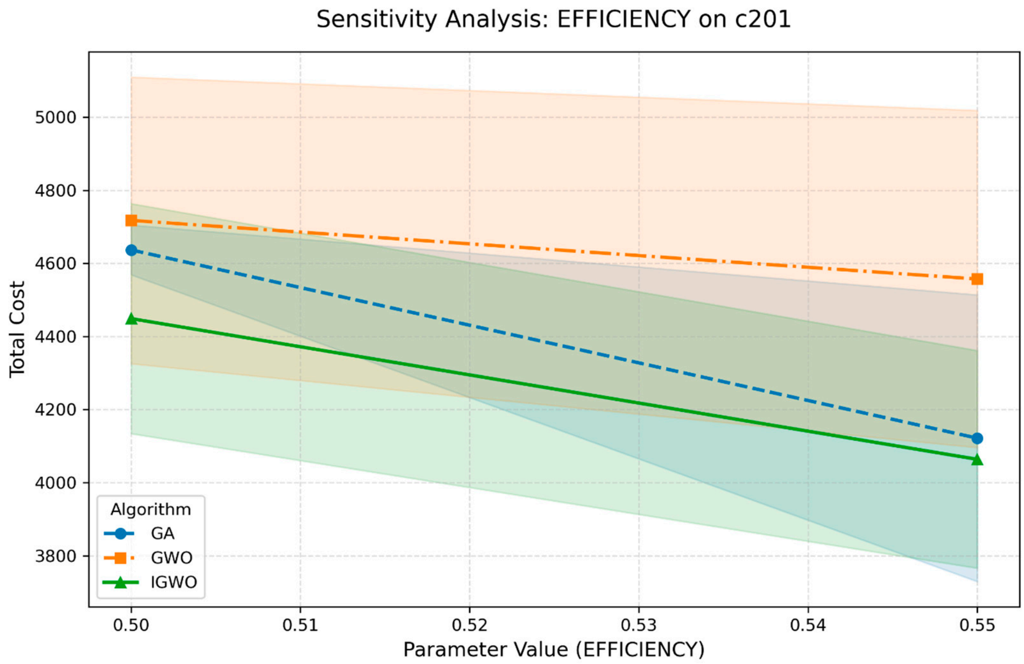

Figure 6. Total Cost and Cost Increase.

Among the three algorithms, IGWO consistently obtains the lowest total cost under both efficiency settings, followed by GA and GWO. This indicates that the proposed IGWO can better adjust route planning and charging decisions when vehicle energy efficiency changes. In particular, when the energy conversion efficiency is relatively low, vehicles face higher energy consumption pressure, and the advantage of IGWO becomes more evident because it can reduce unnecessary detours and improve the coordination between delivery routes and charging decisions.

The shaded areas in the figure indicate the fluctuation range of the results. Compared with GA and GWO, IGWO maintains relatively stable performance while achieving a lower total cost. This suggests that the proposed algorithm has good robustness under different energy efficiency conditions.

Overall, the results indicate that improving energy conversion efficiency can effectively reduce the operating cost of electric cold-chain delivery. For logistics enterprises, improving battery performance, vehicle energy management, and refrigeration system efficiency can help reduce charging demand and total distribution cost.

3.4.3. Effects of Road Gradient, Stop-and-Go Traffic, and Ambient Temperature

To further examine the influence of real-world road and environmental conditions on the operations of electric refrigerated vehicles, a scenario-based sensitivity analysis is conducted. In the revised energy consumption function, road gradient, stop-and-go traffic conditions, and ambient temperature are incorporated to better reflect practical driving conditions. Since the modified Solomon benchmark does not provide real road gradient, traffic interruption, or ambient temperature data, these factors are introduced as scenario-based parameters in the numerical experiments. Four scenarios are designed: baseline, mild, moderate, and severe conditions. The road gradient is set to 0°, 2°, 4°, and 6°, the stop-and-go traffic coefficient is set to 0, 0.1, 0.2, and 0.3, and the ambient temperature is set to 25 °C, 30 °C, 35 °C, and 40 °C, respectively.

For each scenario, the driving energy consumption, refrigeration energy consumption, charging energy, charging frequency, and comparative operating cost are recalculated based on the optimized routes. The comparative operating cost includes fixed vehicle costs, travel costs, charging costs, and refrigeration costs. Since cargo-loss cost and time-window penalty cost are not recalculated in this scenario comparison, the analysis focuses on the marginal effects of road gradient, stop-and-go traffic, and ambient temperature on energy-related operating costs.

Transitioning to the results, harsher road and environmental conditions lead to higher energy consumption for driving and refrigeration. As road gradient, stop-and-go traffic intensity, and ambient temperature increase, vehicles consume more electricity during operation, which further increases charging demand and energy-related operating costs. This confirms the necessity of incorporating road and environmental factors into the energy consumption function of electric refrigerated vehicles.

Figure 7 presents the combined sensitivity analysis of road gradient, stop-and-go traffic conditions, and ambient temperature. As the operating scenario changes from baseline to mild, moderate, and severe conditions, the driving energy consumption, refrigeration energy consumption, charging energy, charging frequency, and comparative operating cost all show an increasing trend. Under the baseline scenario, where the road gradient is 0°, the stop-and-go traffic coefficient is 0, and the ambient temperature is 25 °C, vehicles operate under relatively favorable conditions, resulting in the lowest energy consumption, charging demand, and comparative operating cost. As the road gradient, traffic interruption intensity, and ambient temperature increase simultaneously, vehicles require higher traction energy, greater refrigeration energy, and more frequent or higher-volume charging. This is because a larger road gradient increases the energy required for vehicle movement. Heavier stop-and-go traffic reduces vehicle energy efficiency through frequent acceleration, deceleration, and idling. Additionally, higher ambient temperatures increase the refrigeration load required to maintain cold-chain temperature control. The increase in driving and refrigeration energy consumption further raises charging demand and charging-related costs. These results suggest that electric refrigerated vehicle routing decisions are significantly influenced by real-world road and environmental conditions. Therefore, incorporating road gradient, traffic interruption, and ambient temperature into the energy consumption model can improve the realism and explanatory power of the proposed route optimization framework.

https://doi.org/10.3390/app16104700

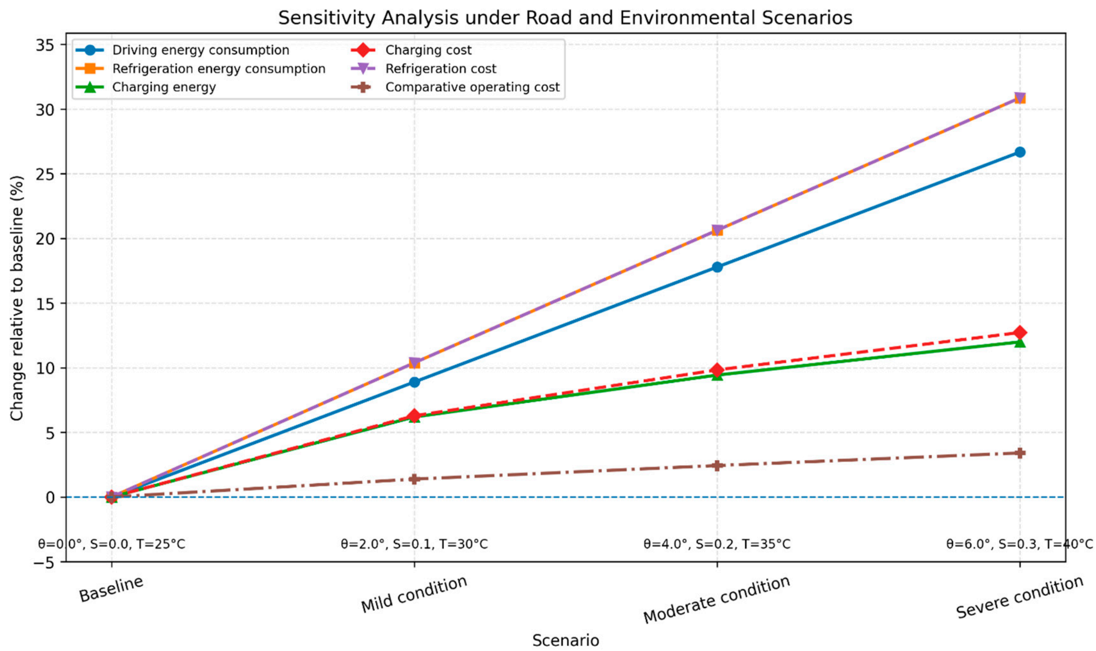

Figure 7. Sensitivity Analysis Combined.

4. Discussion

The results suggest that charging decisions should be jointly optimized with delivery routes in electric cold-chain distribution. Under the mixed public–private charging mode, vehicles can select charging stations based on their route structure, remaining battery level, charging cost, and time-window feasibility. This explains why the mixed charging mode achieves a lower total cost than using only public or private charging stations. It also indicates that charging behavior should not be treated as a separate post-processing step, but as part of the route optimization process.

The comparison of GA, GWO, ALNS, and IGWO further shows that the proposed algorithm is suitable for solving the highly constrained electric refrigerated vehicle routing problem. The improved mechanisms in IGWO, including high-quality initial individual selection, the destroy–repair operator, and the adaptive position update strategy, help improve solution quality and stability. This is particularly important when routing, battery constraints, charging decisions, and cold-chain operation are strongly coupled.

The sensitivity analysis provides practical implications for logistics enterprises. A larger battery capacity can reduce charging frequency and improve route flexibility, but its marginal cost-saving effect gradually decreases. Therefore, battery selection should consider both operational benefits and investment costs. In addition, improving energy conversion efficiency can reduce electricity consumption and charging demand, suggesting that vehicle energy management and refrigeration system efficiency are also important for cost reduction.

Nevertheless, the model still has limitations. The road network is generated from Solomon benchmark coordinates rather than real GIS data, and some traffic and environmental parameters are scenario-based. Future studies can further incorporate real road networks, dynamic traffic information, stochastic customer demand, and more detailed charging-station operation data to improve the realism and scalability of the model.

5. Conclusions

This study investigated the electric refrigerated vehicle routing problem under a mixed public–private charging mode. The model jointly considered vehicle fixed costs, travel costs, charging costs, refrigeration costs, cargo damage costs, and time-window penalty costs, and further incorporated SOC-dependent nonlinear charging, charging-station queuing, and link-based time-dependent travel times.

The C201 case results show that the mixed public–private charging mode achieved the lowest total cost among the three tested charging modes. Specifically, the total cost under the mixed charging mode was 4744.40, compared with 6121.99 under the public-only charging mode and 5024.66 under the private-only charging mode. This result indicates that, in the tested case, allowing vehicles to select both public and private charging stations can reduce total operating cost by improving charging flexibility and reducing charging-related detours and costs.

The algorithm comparison results show that IGWO achieved the best mean objective value in six of the eight tested C-type Solomon instances. For example, in C201, the mean objective value of IGWO was 3331.64 ± 296.78, which was lower than GA, GWO, and ALNS. These results suggest that the high-quality initial population selection, destroy–repair operator, and adaptive position update mechanism can improve the solution quality of the standard GWO under the tested electric cold-chain routing constraints.

The sensitivity analysis provides further evidence on the effects of key operational parameters. When battery capacity increased from 60 kWh to 120 kWh, the total cost decreased, and the number of charging events was reduced. However, the marginal benefit became weaker when battery capacity reached a relatively high level. The analysis of the energy conversion coefficient showed that higher electricity consumption per unit distance increased the total cost by increasing the charging demand. In addition, the scenario-based analysis showed that higher road gradient, stronger stop-and-go traffic intensity, and higher ambient temperature increased driving energy consumption, refrigeration energy consumption, charging energy, charging frequency, and comparative operating cost.

These findings are limited to the tested modified Solomon instances and the scenario-based parameter settings used in this study. The synthetic road network was constructed from benchmark node coordinates rather than real GIS road topology, and the road gradient, traffic, and ambient temperature factors were represented through designed scenarios rather than observed field data. Future studies can incorporate real road networks, dynamic traffic observations, stochastic customer demand, and detailed charging-station operation data to further test the robustness and practical applicability of the proposed model.

Author Contributions: Conceptualization, Y.J. and K.S.; methodology, Y.J.; software, Y.J.; validation, Y.J., K.S. and C.C.; formal analysis, Y.J.; investigation, Y.J.; resources, K.S.; data curation, Y.J.; writing—original draft preparation, Y.J.; writing—review and editing, K.S. and C.C.; visualization, Y.J.; supervision, K.S.; project administration, K.S.; funding acquisition, K.S. All authors have read and agreed to the published version of the manuscript.

Funding: This research received no external funding. The APC was funded by the corresponding author.

Institutional Review Board Statement: Not applicable.

Informed Consent Statement: Not applicable.

Data Availability Statement: The original Solomon benchmark dataset used in this study is publicly available. The customer and depot data from the Solomon C201 instance were retained unchanged. The added charging-station nodes, parameter settings, source code, and experimental results generated in this study have been deposited in a GitHub repository and are available at: https://github.com/Orange092605/EVRP-IGWO, accessed on 7 May 2026.

Conflicts of Interest: The authors declare no conflict of interest.

References

1. The State Council of the People's Republic of China. *Outline of the 15th Five-Year Plan for National Economic and Social Development of the People's Republic of China*; The State Council of the People's Republic of China: Beijing, China, 2026.
2. Xinhua Silk Road. *China's Cold Chain Logistics Industry Boasts Broad Prospects with Listed Companies Accelerating International Expansion*; Xinhua Silk Road: Beijing, China, 2025.
3. Ministry of Agriculture and Rural Affairs of the People's Republic of China. *How Does Cold Chain Enable Fresh Agricultural Products to Travel across Time and Space?* Ministry of Agriculture and Rural Affairs of the People's Republic of China: Beijing, China, 2024.
4. International Energy Agency. *Global EV Outlook 2025: Trends in Heavy-Duty Electric Vehicles*; International Energy Agency: Paris, France, 2025.
5. Chu, Y. *Leading Cities for New Energy Commercial Vehicles in China: 2024*; International Council on Clean Transportation: Washington, DC, USA, 2025.
6. People's Daily Online. *Booming Demand Fuels Growth in China's Cold-Chain Logistics*; People's Daily Online: Beijing, China, 2025.
7. National Energy Administration. *National Electric Vehicle Charging Infrastructure Data in March 2026*; National Energy Administration: Beijing, China, 2026.
8. National Development and Reform Commission; National Energy Administration; Ministry of Industry and Information Technology; Ministry of Housing and Urban-Rural Development; Ministry of Transport; State Administration for Market Regulation. *Three-Year Action Plan for Doubling EV Charging Service Capacity (2025–2027)*; National Development and Reform Commission (NDRC): Beijing, China, 2025.
9. Wang, S.; Tao, F.; Shi, Y.; Wen, H. Optimization of Vehicle Routing Problem with Time Windows for Cold Chain Logistics Based on Carbon Tax. *Sustainability* **2017**, *9*, 694. [CrossRef]
10. Lee, E.H.; Stoeltje, G. How Far Does Your Food Travel on the Highway? Food Miles and Carbon Footprint. *J. Clean. Prod.* **2025**, *518*, 145915. [CrossRef]
11. Maggini, M.; Loreti, G.; Santoni, F.; Facci, A.L.; Ubertini, S.; Cigolotti, V.; Monteleone, G. Technical Assessment and Economic Analysis of Zero-Carbon Freight Road Transportation Vehicles. *Int. J. Hydrogen Energy* **2026**, *212*, 153707. [CrossRef]
12. He, M.; Yang, M.; Fu, W.; Wu, X.; Izui, K. Optimization of Electric Vehicle Routes Considering Multi-Temperature Co-Distribution in Cold Chain Logistics with Soft Time Windows. *World Electr. Veh. J.* **2024**, *15*, 80. [CrossRef]
13. Kim, G. Electric Vehicle Routing Problem with States of Charging Stations. *Sustainability* **2024**, *16*, 3439. [CrossRef]
14. Nasri, S.; Mansouri, N.; Mnassri, A.; Lashab, A.; Vasquez, J.; Rezk, H. Global Analysis of Electric Vehicle Charging Infrastructure and Sustainable Energy Sources Solutions. *World Electr. Veh. J.* **2025**, *16*, 194. [CrossRef]
15. Gan, Z.; Dong, P.; Fu, Z.; Ju, Y.; Shen, Y. Optimizing Electric Cold-Chain Vehicle Scheduling for Sustainable Urban Logistics: A Novel Framework Balancing Freshness and Vehicle Charging. *Energies* **2025**, *18*, 1705. [CrossRef]
16. Cortés-Murcia, D.L.; Prodhon, C.; Afsar, H.M. The electric vehicle routing problem with time windows, partial recharges and satellite customers. *Transp. Res. Part E Logist. Transp. Rev.* **2019**, *130*, 184–206. [CrossRef]
17. Zhou, Y.; Lei, Q.; Li, L.; Wu, Z. An Overview of Energy Replenishment Strategies for the Electric Vehicle Routing Problem: Models and Solution Algorithms. *Energies* **2025**, *18*, 6196. [CrossRef]
18. Erdelić, T.; Carić, T. Goods Delivery with Electric Vehicles: Electric Vehicle Routing Optimization with Time Windows and Partial or Full Recharge. *Energies* **2022**, *15*, 285. [CrossRef]
19. Schneider, M.; Stenger, A.; Goeke, D. The Electric Vehicle-Routing Problem with Time Windows and Recharging Stations. *Transp. Sci.* **2014**, *48*, 500–520. [CrossRef]
20. Keskin, M.; Çatay, B. Partial Recharge Strategies for the Electric Vehicle Routing Problem with Time Windows. *Transp. Res. Part C Emerg. Technol.* **2016**, *65*, 111–127. [CrossRef]
21. Hiermann, G.; Puchinger, J.; Røpke, S.; Hartl, R.F. The Electric Fleet Size and Mix Vehicle Routing Problem with Time Windows and Recharging Stations. *Eur. J. Oper. Res.* **2016**, *252*, 995–1018. [CrossRef]
22. Yu, V.F.; Anh, P.T.; Chen, Y.-W. The Electric Vehicle Routing Problem with Time Windows, Partial Recharges, and Parcel Lockers. *Appl. Sci.* **2023**, *13*, 9190. [CrossRef]
23. Zhao, J.; Zeng, Z.; Liu, Y. Electric Vehicle Routing Problem Considering Traffic Conditions and Real-Time Loads. *Transp. Res. Part C Emerg. Technol.* **2025**, *176*, 105150. [CrossRef]
24. Ding, N.; Yang, J.; Han, Z.; Hao, J. Electric-Vehicle Routing Planning Based on the Law of Electric Energy Consumption. *Mathematics* **2022**, *10*, 3099. [CrossRef]
25. Abid, M.; Tabaa, M.; Hachimi, H. Electric Vehicle Routing Problem with an Enhanced Vehicle Dispatching Approach Considering Real-Life Data. *Energies* **2024**, *17*, 1596. [CrossRef]
26. Zuo, X.; Xiao, Y.; You, M.; Kaku, I.; Xu, Y. A New Formulation of the Electric Vehicle Routing Problem with Time Windows Considering Concave Nonlinear Charging Function. *J. Clean. Prod.* **2019**, *236*, 117687. [CrossRef]
27. Wang, D.; Zheng, W.; Zhou, H. Robust Optimization for Electric Vehicle Routing Problem Considering Time Windows under Energy Consumption Uncertainty. *Appl. Sci.* **2025**, *15*, 761. [CrossRef]

28. Zhang, S.; Gajpal, Y.; Appadoo, S.S.; Abdulkader, M.M.S. Electric Vehicle Routing Problem with Recharging Stations for Minimizing Energy Consumption. *Int. J. Prod. Econ.* **2018**, *203*, 404–413. [CrossRef]
29. Wang, Y.; Zhou, J.; Sun, Y.; Wang, X.; Zhe, J.; Wang, H. Electric Vehicle Charging Station Location-Routing Problem with Time Windows and Resource Sharing. *Sustainability* **2022**, *14*, 11681. [CrossRef]
30. Dong, H.; Luo, Z.; Huang, N.; Hu, H.; Qin, H. The Electric Vehicle Dial-a-Ride Problem: Integrating Ride-Sharing and Time-of-Use Electricity Pricing. *Transp. Res. Part E Logist. Transp. Rev.* **2025**, *194*, 103946. [CrossRef]
31. Raeesi, R.; Zografos, K.G. The Electric Vehicle Routing Problem with Time Windows and Synchronised Mobile Battery Swapping. *Transp. Res. Part B Methodol.* **2020**, *140*, 101–129. [CrossRef]
32. Kullman, N.D.; Goodson, J.C.; Mendoza, J.E. Electric Vehicle Routing with Public Charging Stations. *Transp. Sci.* **2021**, *55*, 637–659. [CrossRef]
33. Cataldo-Díaz, C.; Linfati, R.; Escobar, J.W. Mathematical Model for the Electric Vehicle Routing Problem Considering the State of Charge of the Batteries. *Sustainability* **2022**, *14*, 1645. [CrossRef]
34. Qi, B.; Li, G. The evolution of the cold chain logistics vehicle routing problem: A bibliometric and visualization review. *Digit. Transp. Saf.* **2024**, *3*, 92–114. [CrossRef]
35. Jiang, X.; Liu, X.; Pan, F.; Han, Z. Optimizing Cold Chain Distribution Routes Considering Dynamic Demand: A Low-Emission Perspective. *Sustainability* **2024**, *16*, 2013. [CrossRef]
36. Liu, G.; Hu, J.; Yang, Y.; Xia, S.; Lim, M.K. Vehicle Routing Problem in Cold Chain Logistics: A Joint Distribution Model with Carbon Trading Mechanisms. *Resour. Conserv. Recycl.* **2020**, *156*, 104715. [CrossRef]
37. Huang, G.; Qi, Y.; Cai, Y.; Luo, Y.; Huang, H. A Grey Wolf Optimizer Algorithm for Multi-Objective Cumulative Capacitated Vehicle Routing Problem Considering Operation Time. *Biomimetics* **2024**, *9*, 331. [CrossRef]
38. Aslan Yıldız, Ö.; Sarıçiçek, İ.; Yazıcı, A. A Reinforcement Learning-Based Solution for the Capacitated Electric Vehicle Routing Problem from the Last-Mile Delivery Perspective. *Appl. Sci.* **2025**, *15*, 1068. [CrossRef]
39. Wu, Z.; Lou, P.; Hu, J.; Zeng, Y.; Fan, C. An Adaptive Large Neighborhood Search for a Green Vehicle Routing Problem with Depot Sharing. *Mathematics* **2025**, *13*, 214. [CrossRef]
40. Shi, J.; Li, Z.; Wei, Y.; Huang, X.; Gao, S. A Novel Multi-Objective Optimization Model of Electric Vehicles' Path Planning and Charging Scheduling Based on Users' Comprehensive Satisfaction. *Proc. Inst. Mech. Eng. Part I J. Syst. Control Eng.* **2025**. *onlinefirst*. [CrossRef]
41. Bruglieri, M.; Paolucci, M.; Pisacane, O. A Matheuristic for the Electric Vehicle Routing Problem with Time Windows and a Realistic Energy Consumption Model. *Comput. Oper. Res.* **2023**, *157*, 106261. [CrossRef]
42. Yin, L.; Zhu, R.; Jian, D. Research on Green Distribution Problems of Mixed Fleets Considering Multiple Charging Methods. *Energies* **2025**, *18*, 5220. [CrossRef]
43. Han, H.; Chen, L.; Fang, S.; Liu, Y. The Routing Problem for Electric Truck with Partial Nonlinear Charging and Battery Swapping. *Sustainability* **2023**, *15*, 13752. [CrossRef]
44. Fan, L.; Liu, C.; Dai, B.; Li, J.; Wu, Z.; Guo, Y. Electric Vehicle Routing Problem Considering Energy Differences of Charging Stations. *J. Clean. Prod.* **2023**, *418*, 138184. [CrossRef]
45. He, Y. Research on the Electric Vehicle Routing Problem Considering Power Consumption Rate. Master's Thesis, Nanjing University, Nanjing, China, 2021.